JOURNAL OF SOLID STATE CHEMISTRY **127,** 315–324 (1996)
ARTICLE NO. 0389

New Copper Oxychlorides $Ca_4Ln_2Cu_3O_8Cl_4$, First Members of the Intergrowth Series $(Ca_2CuO_2Cl_2)_m(Ln_2Ca_2Cu_2O_6Cl_2)_n$ (Ln = Gd, Sm)

D. Pelloquin, A. Sundaresan, M. Hervieu, C. Michel, and B. Raveau

Laboratoire CRISMAT, ISMRA et Université de Caen, URA 1318 associée au CNRS, Boulevard du Maréchal Juin, 14050 Caen Cedex, France

Received June 27, 1996; in revised form September 16, 1996; accepted September 18, 1996

The oxychlorides $Ca_4Ln_2Cu_3O_8Cl_4$, with Ln = Gd and Sm, intergrowths of the T and T* structures have been synthesized for the first time. The HREM study, coupled with EDS analysis, shows that the actual composition of these phases is significantly different from the ideal composition, due to the presence of complex nonstoichiometry phenomena involving the formation of intergrowth defects corresponding to other members with the general formulation $(Ca_2CuO_2Cl_2)_m(Ln_2Ca_2Cu_2O_6Cl_2)_n$. Moreover, substitutions on the anionic and cationic sites are also evidenced. These results demonstrate the high flexibility of the oxychloride layer structure and suggest the possibility to isolate new members in this structural series.

INTRODUCTION

The recent discovery of superconductivity in copper oxyhalides (1, 2) has opened a new family of superconductors. The synthesis of the oxychlorides, $A_2CuO_2Cl_2$ (3) and more recently $ALnCuO_3Cl$ with A = Ca, Sr where Ln is a lanthanide (4), shows that the chlorine occupies the apical positions formed either by the CuO_6 octahedra or by the CuO_5 pyramids. The former, $A_2CuO_2Cl_2$, exhibits indeed the La_2CuO_4-type structure, named T; i.e., they consist of infinite single perovskite layers $[ACuO_2Cl]_\infty$ intergrown with single rock salt (RS) layers $[ACl]_\infty$ (Fig. 1a), whereas the latter $ALnCuO_3Cl$ belongs to the $Nd_{2.64}Sr_{0.82}Ce_{0.54}Cu_2O_8$-type structure (Fig. 1c), named T*. That is, they are built up of double pyramidal copper layers separated by double fluorite layers, with the formulation $[ALn_2Cu_2O_6Cl]_\infty$, intergrown with single rock salt layers $[ACl]_\infty$. Both series of oxychlorides have, in common, the existence of $[ACl]_\infty$ rock salt layer so that it should be possible to build intergrowths of these two structures by varying the ratios Ca/Ln and O/Cl in the system Ca–Ln–Cu–O–Cl. We report herein on the synthesis and structure of new oxychlorides $Ca_4Ln_2Cu_3O_8Cl_4$, with Ln = Gd, Sm that correspond to the first member ($m = n = 1$) of the structural family $(Ca_2CuO_2Cl_2)_m(Ln_2Ca_2Cu_2O_6Cl_2)_n$.

EXPERIMENTAL

The $Ca_4Ln_2Cu_3O_8Cl_4$ copper oxychloride was synthesized by solid-state chemical reaction, from oxides CaO, Ln_2O_3, CuO and hydrated copper chloride $CuCl_2, 2H_2O$ as previously mentioned for $CaLnCuO_3Cl$ (4). The latter phase with Ln = Gd, which was used as reference for an HREM study, was also synthesized in our study. For both phases, an excess of alkaline earth and chloride was always necessary to stabilize the structures as previously mentioned (4). All the precursors were weighed accurately to respect the nominal compositions, $Ca_{4.4}Ln_{1.6}Cu_3Cl_{5.6}O_7, 2.8H_2O$ and $Ca_{1.5}LnCuCl_2O_3, 2H_2O$, respectively, and mixed thoroughly. Then the mixtures were placed in an alumina crucible and calcined in air at 700°C for about 2 h. The products were reground and pressed into bars. The bars were sintered at 750 and 800°C for 12 h, respectively.

The purity and of the samples were checked by electron diffraction (ED) on more than 50 microcrystals for each sample, using a JEOL 200Cx electron microscope, fitted with an eucentric goniometer (±60°), equipped with an EDX analyzer.

The cell parameters were refined from powder X-ray diffraction (XRD) data, collected with a Philips diffractometer (CuK_α radiation) in the range $3° < 2\theta < 120°$, using the program Fullprof (5). The high resolution electron microscopy (HREM) was performed with a TOPCON 02B, operating at 200 kV and having a resolution of 1.8 Å, and image simulations were carried out with the MacTempas multislice program.

RESULTS AND DISCUSSION

For the above-mentioned experimental conditions, two new phases, $Ca_4Ln_2Cu_3O_8Cl_4$ with Ln = Gd and Sm have been synthesized. The powder XRD patterns of these black compounds show close relationship with the $CaLnCuO_3Cl$ phase (4) as shown, for instance, for Ln = Gd (Fig. 2a). Nevertheless, one observes two other phases, namely $Ca_2CuO_2Cl_2$ and $CaGdCuO_3Cl$, as impurities besides the ma-

0022-4596/96 $18.00

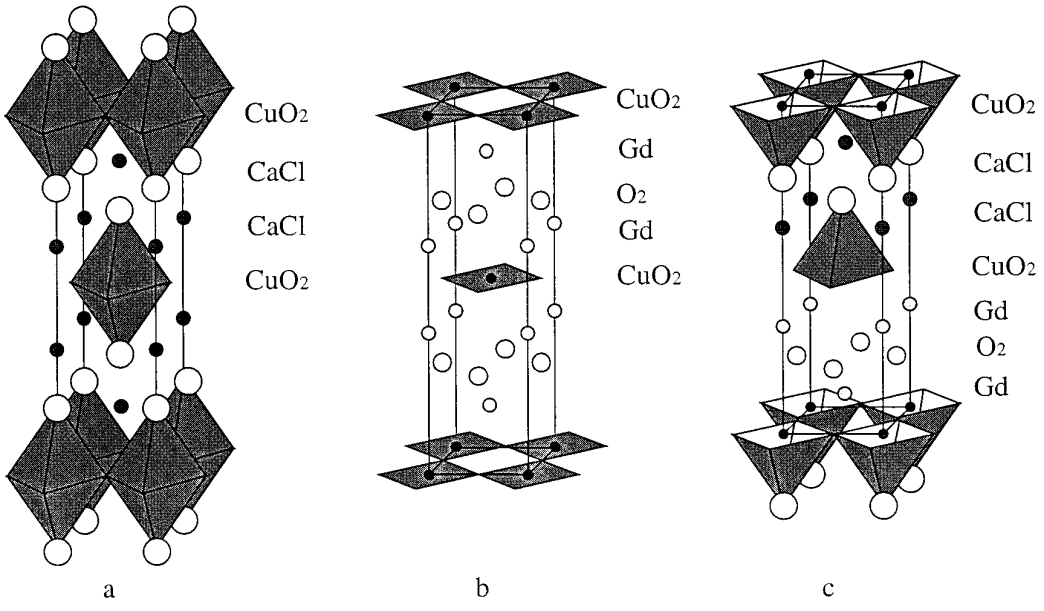

FIG. 1. Schematic representation of the structure of (a) $Ca_2CuO_2Cl_2$ (T structure), (b) Gd_2CuO_4 (T′ structure), and (c) $CaGdCuO_3Cl$ (T* structure). The chlorine occupies the apical positions of the octahedra or pyramids.

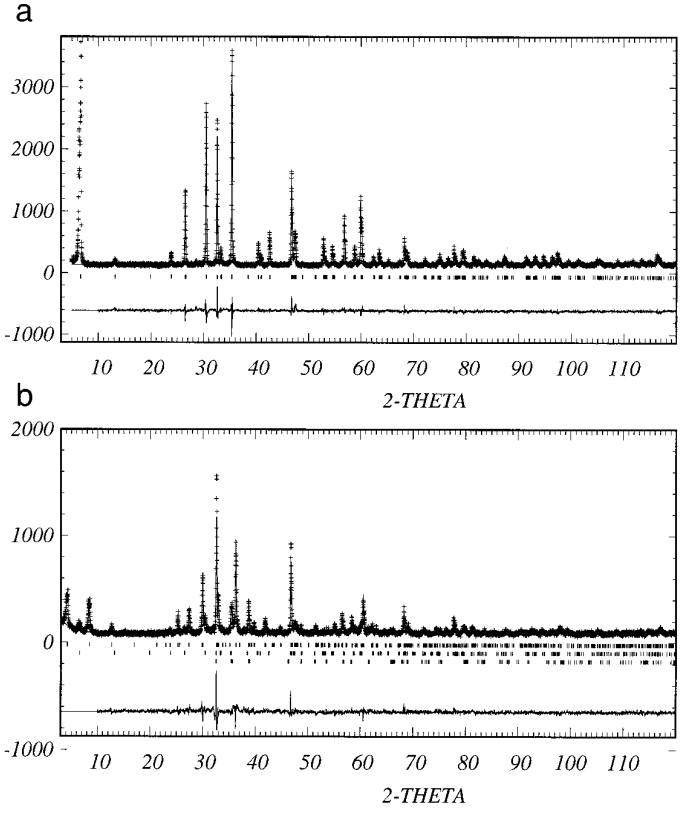

FIG. 2. Experimental (crosses), calculated (line), and difference profiles obtained from a Rietveld refinement of the powder XRD data for (a) $CaGdCuO_3Cl$ and (b) $Ca_4Gd_2Cu_3O_8Cl_4$. The allowed reflection positions are shown by the vertical tick marcks. In the case of (b), the impurity phases are $CaGdCuO_3Cl$ and CuO, respectively.

jor phase. However, the presence of one intense peak around 21 Å suggests an intergrowth between the two structures, $Ca_2CuO_2Cl_2$ (T) and $CaGdCuO_3Cl$ (T*), corresponding to the ideal formula $Ca_4Gd_2Cu_3O_8Cl_4$. Such a hypothesis is also supported by the reconstruction of the reciprocal space from the [001], [100], and [110] ED patterns (Fig. 3) that evidence the reflection condition, (hkl) $h + k + l = 2n$, characteristic of an I-type space group with $a \approx a_p$ and $c \approx 42$ Å.

The powder XRD patterns can then be indexed (Table 1) in the space group $I4/mmm$ with the parameters

$a = 3.8865\ (1)$ Å and $c = 41.827\ (2)$ Å for Ln = Gd

$a = 3.8884\ (1)$ Å and $c = 41.825\ (2)$ Å for Ln = Sm.

On the basis of these observations a structural model that consists of the stacking of single $[Ca_2Ln_2Cu_2O_6Cl_2]$ layers that are 13.5 Å thick, with single $[Ca_2CuO_2Cl_2]$ layers that are 7.5 Å thick, can be proposed as shown in Fig. 4.

In order to confirm this model, structure calculations were performed from the powder XRD data for $Ca_4Gd_2Cu_3O_8Cl_4$ using a Rietveld method. The initial atomic coordinates were estimated from the model described in Fig. 4, using the space group $I4/mmm$ (no. 139). The refinement of the atomic coordinates of the heavy elements Ca, Gd, Cu, and Cl confirmed the validity of the model. Then the positions of the oxygen atoms and the isotropic thermal factor of all the atoms (except for oxygen for which B was fixed at 1 Å^2) were successively refined. At this stage, the R_i factor could not be lowered below 0.12, and abnormal B factors were observed for two sites labeled Ca(1) and Cl(2). The composition of the microcrystals, deduced from

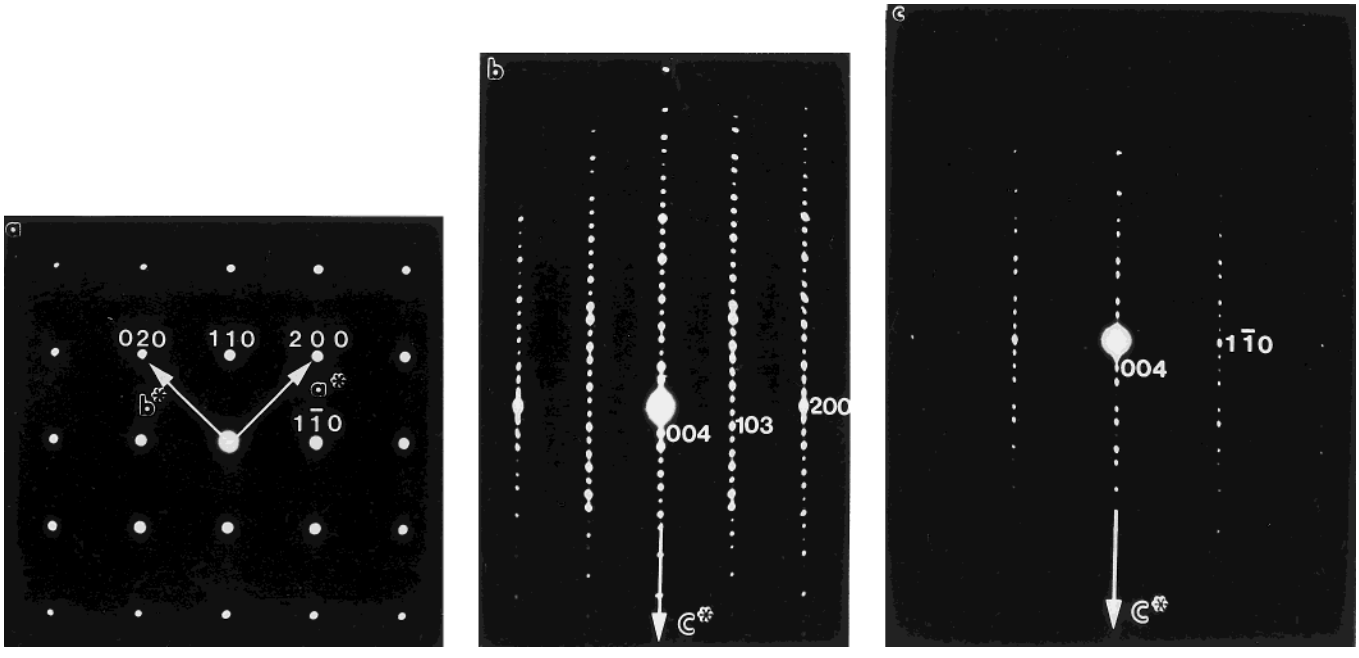

FIG. 3. [001], [100], and [110] ED patterns of $Ca_4Gd_2Cu_3O_8Cl_4$.

TABLE 1
Indexation of the X-Ray Diffraction Pattern (for $3° \leq 2\theta \leq 50°$) Corresponding to $Ca_4Gd_2Cu_3O_8Cl_4$ Sample

d_{obs}	d_{calc}	$2\theta_{calc}$	I/I_0	h	k	l
20.89	20.91	4.222	20.9	0	0	2
10.44	10.45	8.449	19.0	0	0	4
6.971	6.971	12.688	5.5	0	0	6
3.863	3.869	22.963	1.0	1	0	1
3.737	3.744	23.747	3.2	1	0	3
3.524	3.525	25.247	13.5	1	0	5
3.252	3.258	27.352	18.0	1	0	7
2.981	2.981	29.947	45.0	1	0	9
2.748	2.748	32.556	100	1	1	0
2.727	2.725	32.843	4.0	1	1	2
2.720	2.718	32.928	19.0	1	0	11
2.660	2.658	33.694	5.0	1	1	4
2.616	2.614	34.275	3.0	0	0	16
2.477	2.478	36.216	67.1	1	0	13
2.324	2.324	38.719	22.0	0	0	18
2.268	2.265	39.753	7.6	1	0	15
2.159	2.158	41.825	10.3	1	1	12
2.092	2.091	43.225	1.0	0	0	20
2.023	2.022	44.772	4.6	1	1	14
1.944	1.943	46.706	72.0	2	0	0
1.913	1.915	47.425	1.0	1	0	19
				2	0	4
1.902	1.901	47.803	6.0	0	0	22
				1	1	16
1.871	1.872	48.599	5.5	2	0	6

the EDS analysis, showed that the actual composition "$Ca_{3.7}Gd_{2.3}Cu_{3.1}Cl_{3.8}$" was significantly different from the ideal composition. This suggested the presence of extended defects, in the structure, due to the random intergrowth mechanisms; such defects, which were shown latter by HREM, could be taken into consideration in the calculations by refining the occupancy factors of the Ca(1) and Cl(2) sites. The R_i factor could then be lowered to 0.089, for an occupancy of the Ca(1) site by 10% gadolinium and of the Cl(2) site by 8% oxygen.

The atomic parameters obtained for oxygens (Table 2), although they cannot be considered as accurate, lead how-

TABLE 2
$Ca_4Gd_2Cu_3O_8Cl_4$: Atomic Parameters

Atom	Site	x	y	z	B_{iso} (Å^2)	τ
(Ca/Gd)(1)	4e	0	0	0.4611 (4)	0.0 (7)	0.90/0.10 (2)
Ca(2)	4e	0	0	0.1428 (4)	0.0 (5)	1
Gd(2)	4e	0	0	0.2219 (2)	0.7 (1)	1
Cu(1)	2a	0	0	0	0.9 (7)	1
Cu(2)	4e	0	0	0.3221 (3)	0.1 (4)	1
O(1)	4e	0	1/2	0	1.0[a]	1
O(2)	8g	0	1/2	0.319 (1)	1.0[a]	1
O(3)	4d	0	1/2	1/4	1.0[a]	1
Cl(1)	4e	0	0	0.0644 (5)	0.0 (5)	1
(Cl/O)(2)	4e	0	0	0.3824 (5)	2.1 (6)	0.92/0.08 (4)

Space group: $I4/mmm$ (n°139) $\quad \chi^2 = 2.54$
$a = 3.8865$ (1) Å $\quad R_i = 0.089$
$c = 41.827$ (2) Å

[a] Value fixed arbitrarely.

TABLE 3
$Ca_4Gd_2Cu_3O_8Cl_4$: Interatomic Distances

(Ca/Gd)(1)–Cl(1) × 4	2.946 (8) Å	Gd(2)–O(2) × 4	2.60 (3) Å
(Ca/Gd)(1)–O(1) × 4	2.53 (1) Å	Gd(2)–O(3) × 4	2.269 (4) Å
(Ca/Gd)(1)–(Cl/O)(2) × 1	3.30 (2) Å	Cu(1)–O(1) × 4	1.943 (1) Å
Ca(2)–(Cl/O)(2) × 4	2.939 (9) Å	Cu(1)–Cl(1) × 2	2.68 (2) Å
Ca(2)–Cl(1) × 1	3.28 (3) Å	Cu(2)–O(2) × 4	1.947 (3) Å
Ca(2)–O(2) × 4	2.52 (3) Å	Cu(2)–(Cl/O)(2) × 1	2.51 (2) Å

ever to interatomic distances (Table 3) that are consistent with the different bond distances observed in the parent structures $Ca_2CuO_2Cl_2$ and $CaGdCuO_3Cl$ (Table 4). It is to be noted that only the Cu(2)–Cl(2) distances are quite short (2.5 Å) compared to those usually observed (2.7 Å); this can be explained by the fact that it represents only an average distance, intermediate between the Cu–Cl and Cu–O bonds, the Cl(2) site being partially occupied by oxygen.

The relatively high reliability factors obtained from XRD data did not allow the structure to be definitely established. Moreover, the origin of the ''statistical distribution'' of oxygen over the Cl(2) sites had to be answered. For these reasons, a HREM study was absolutely necessary.

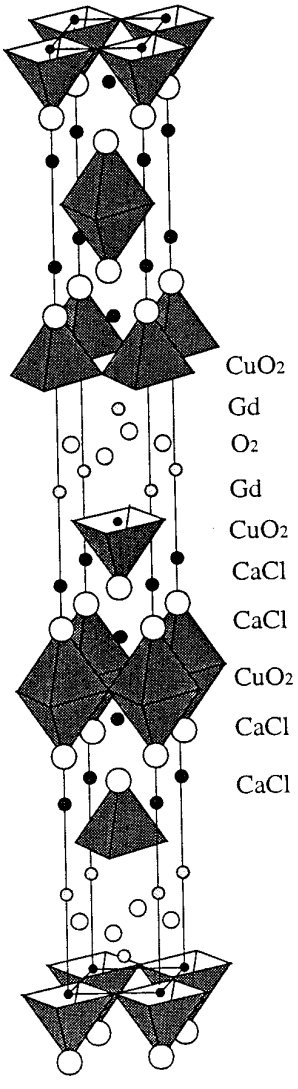

FIG. 4. Idealized drawing of the proposed structure for $Ca_4Gd_2Cu_3O_8Cl_4$.

HREM STUDY

In order to get a better understanding of the order–disorder phenomena which take place in such materials, the image contrast of a parent structure, the T* phase $CaGdCuO_3Cl$, was chosen as reference.

1. $CaGdCuO_3Cl$

The structure of the oxychloride $CaSmCuO_3Cl$ was previously established from single crystal data by Ramanujachary *et al.* (6). For the gadolinium-based compound (this work), the refined positional parameters are very close to Sm-based structure [6]. Image calculations were carried out with these atomic positions.

The ED investigation confirms the cell parameters and symmetry of this phase, i.e., $a \approx a_p$ and $c \approx 13.4$ Å (Fig. 5a) and attests the good crystallinity of the sample. The EDS analyses show that most of the crystals exhibit an actual composition close to the nominal one, i.e., a ratio

TABLE 4
Interatomic Distances

$Ca_2CuO_2Cl_2$ Ref. (3)		$CaGdCuO_3Cl$	
Cu–O × 4	1.93 Å	Cu–O(1) × 4	1.943 (1) Å
Cu–Cl × 2	2.73 Å	Cu–Cl × 2	2.747 (9) Å
Ca–O × 4	2.49 Å	Ca–O(1) × 4	2.452 (8) Å
Ca–Cl × 4	2.98 Å	Ca–Cl × 4	2.994 (4) Å
Ca–Cl × 1	3.19 Å	Ca–Cl × 1	3.170 (9) Å
		Gd–O(1) × 4	2.667 (1) Å
		Gd–O(2) × 4	2.277 (1) Å

1/1/1/1 for Ca/Gd/Cu/Cl. The [100] HREM images are the best suited for the layers' identification and the visualization of their stacking. Two typical structure images selected from the through focus series are displayed in Figs. 5b and 5c; the corresponding enlarged calculated image is shown besides the micrograph for comparison. In the first image (Fig. 5b) the high electron density zones appear as bright dots, and the contrast on the crystal edge can be easily described by considering three types of layers. The first type corresponds to a group of two layers which exhibits a well-known contrast, usually observed in the superconducting cuprates containing double fluorite layers (7); it consists of two adjacent rows of staggered bright dots, 2.4 Å spaced, which are correlated to the double $[Gd_2O_2]_\infty$ layers (indicated by small black triangles). The second type corresponds to a group of four rows, very close together, of staggered small gray dots. These rows are correlated to the layer sequence [Ca]–[Cl]–[Cl]–[Ca], and are generated by the positions of chlorine within the double $[Ca_2Cl_2]_\infty$ layers. This second group is indicated in the image by curved arrows and its overall width, i.e., the distance between the two extreme [Ca] layers which is close to 4.4 Å, is indicated by an horizontal dash. The third type consists of a single row of bright dots correlated to the $[CuO_2]_\infty$ layers (indicated by the larger black triangles). The $[Ca_2Cl_2]_\infty$ and $[Gd_2O_2]_\infty$ slabs are systematically separated by a single $[CuO_2]_\infty$ layer so that the experimental sequence fits well with that expected for the parent $CaGdCuO_3Cl$ structure. This contrast is also in agreement with that calculated for a focus value of −550 Å and a crystal thickness close to 30 Å. The second image (Fig. 5c) is recorded for a focus value close to −250 Å (Scherzer value) where the cation positions appear as dark dots. The prominent feature of the image contrast arises from the double $[Ca_2Cl_2]_\infty$ layers which appear as very bright zigzag lines. In the thicker part of the crystal, where the contrast can no longer be directly correlated to the atom positions, the chlorine layers still appear as bright lines.

In a general way, one observes an even contrast at the level of the gadolinium and copper layers, whereas it often appears disturbed at the level of the $[Ca_2Cl_2]_\infty$ layers. This point will be discussed further.

2. $Ca_4Gd_2Cu_3O_8Cl_4$

The HREM images, recorded along [100] as well as along [110], confirm the structural model proposed for the new oxychloride (Fig. 4), i.e., a regular intergrowth between the layers $[Ca_2CuO_2Cl_2]$ and $[Ca_2Gd_2Cu_2O_6Cl_2]$.

A [100] HREM image were the cations are imaged as dark dots is given in Fig. 6a and compared (in inset) with the enlarged simulated images, calculated for a focus value close to −250 Å and three values of crystal thickness (15, 30, and 45 Å). These calculations show that, in agreement with the experimental images, the two rows of staggered bright dots are correlated with the low electron density zones between the gadolinium atoms in the double $[Gd_2O_2]_\infty$ layers (indicated by small black triangles); one also observes two groups of adjacent rows of staggered bright dots, scarcely resolved, correlated to the low electron density zones between the chlorine atoms in the $[Ca_2Cl_2]_\infty$ layers. When the crystal thickness increases, the prominent contrast remains in the bright rows of the $[Ca_2Cl_2]_\infty$ layers. This feature provides an efficient way to characterize the layer stacking mode.

A [110] HREM image is shown in Fig. 6b, where the high density zones are highlighted (focus value close to −550 Å). The contrast mainly consists of two groups of double rows of elongated bright dots, about 4.4 Å apart. The latter are correlated to the superposition of the calcium and chlorine atoms which are projected over two close positions along that direction (indicated by curved arrows); the enlarged image calculated for such a focus value is shown in inset in the bottom part of the image. The gadolinium positions appear as two rows of small gray dots (small black triangles). This contrast is not strongly modified when the crystal thickness increases.

3. Structural Defects

The HREM investigation of the two samples, $Ca_2Gd_2Cu_2O_6Cl_2$ and $Ca_4Gd_2Cu_3O_8Cl_4$, shows that two types of defects are mainly observed in these materials.

Intergrowth defects: The members $(Ca_2CuO_2Cl_2)_m(Ca_2Gd_2Cu_2O_6Cl_2)_n$. The existence of stacking defects was detected in both matrices; they could be expected in such phases since they are based on the intergrowth principle and belong to a single system, *Ln*–Ca–Cu–O–Cl. Thus, these defects are very classical in such materials and correspond to the formation of intergrowths with the generic formula $(Ca_2CuO_2Cl_2)_m(Ca_2Ln_2Cu_2O_6Cl_2)_n$. In that way, $Ca_4Gd_2Cu_3O_8Cl_4$ members are observed as defective members in the $Ca_2Gd_2Cu_2O_6Cl_2$ phase and vice versa. The crystals of the two phases are generally almost regular with only a few isolated defects but, sometimes, true mixed crystals corresponding to the coexistence of the members $Ca_2Gd_2Cu_2O_6Cl_2$ ($m = 0$; $n = 1$) and $Ca_4Gd_2Cu_3O_8Cl_4$ ($m = 1$; $n = 1$) in the form of large domains are observed. In such mixed crystals, the EDS analyses show a significant variation of the atomic ratios and, moreover, streaks are observed along c^* in ED patterns as shown in Figs. 7a and 7b. This is also seen in the HREM image shown in Fig. 7c, where the major structure is $Ca_4Gd_2Cu_3O_8Cl_4$ on the left part of the image and is $Ca_2Gd_2Cu_2O_6Cl_2$ on the right part.

Higher members of the family are also locally formed. For example, ($m = 2$; $n = 1$) members, $(Ca_2CuO_2Cl_2)_2(Ca_2Gd_2Cu_2O_6Cl_2)_1$, take place in the ($m = 1$; $n =$

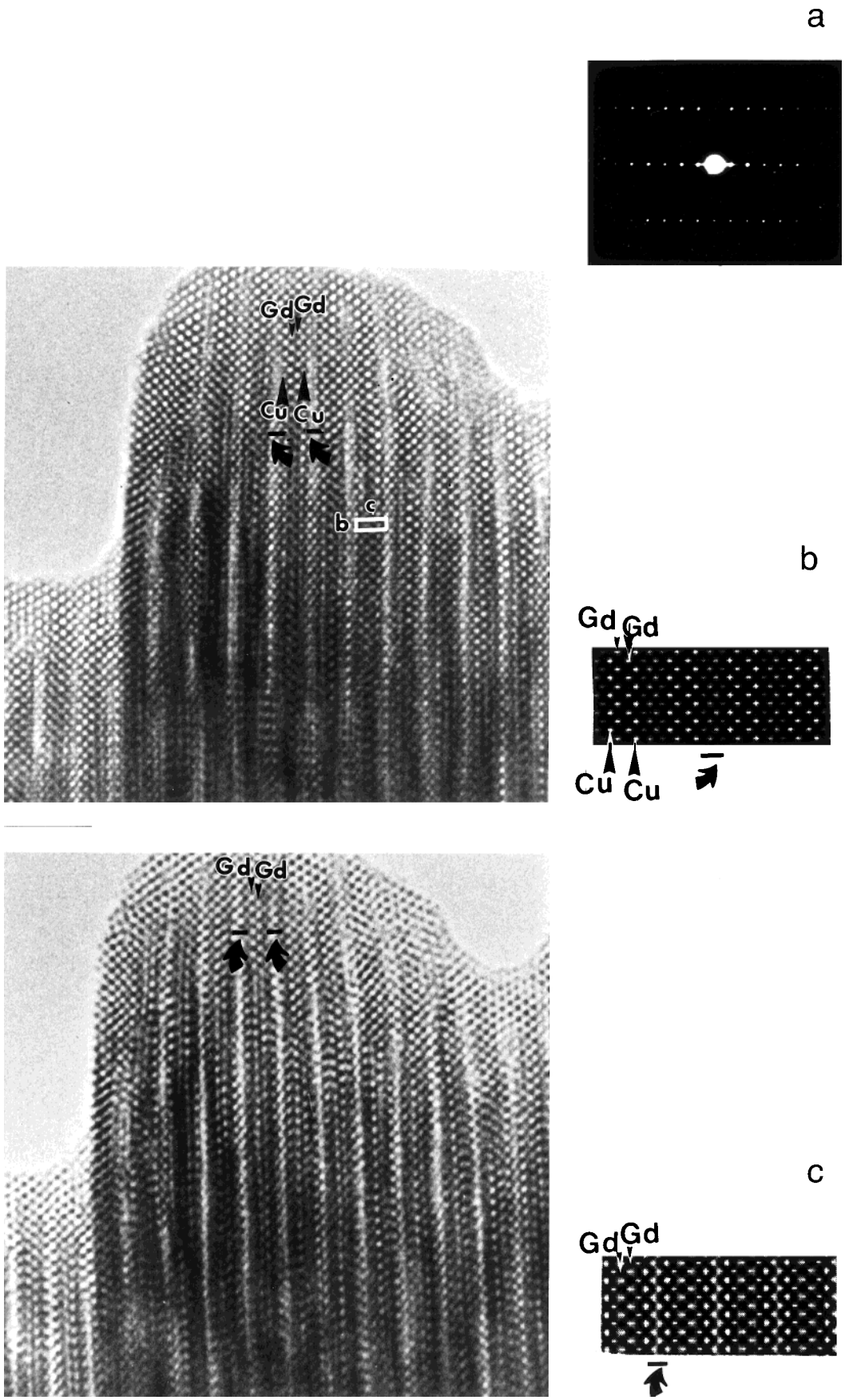

FIG. 5. (a) [100] ED pattern of $CaGdCuO_3Cl$. (b, c) [100] HREM images of $CaGdCuO_3Cl$ with different focus values. In (b), the high electron density zones appear as bright dots and in (c) it appears as dark dots. Calculated images are also shown besides the respective images.

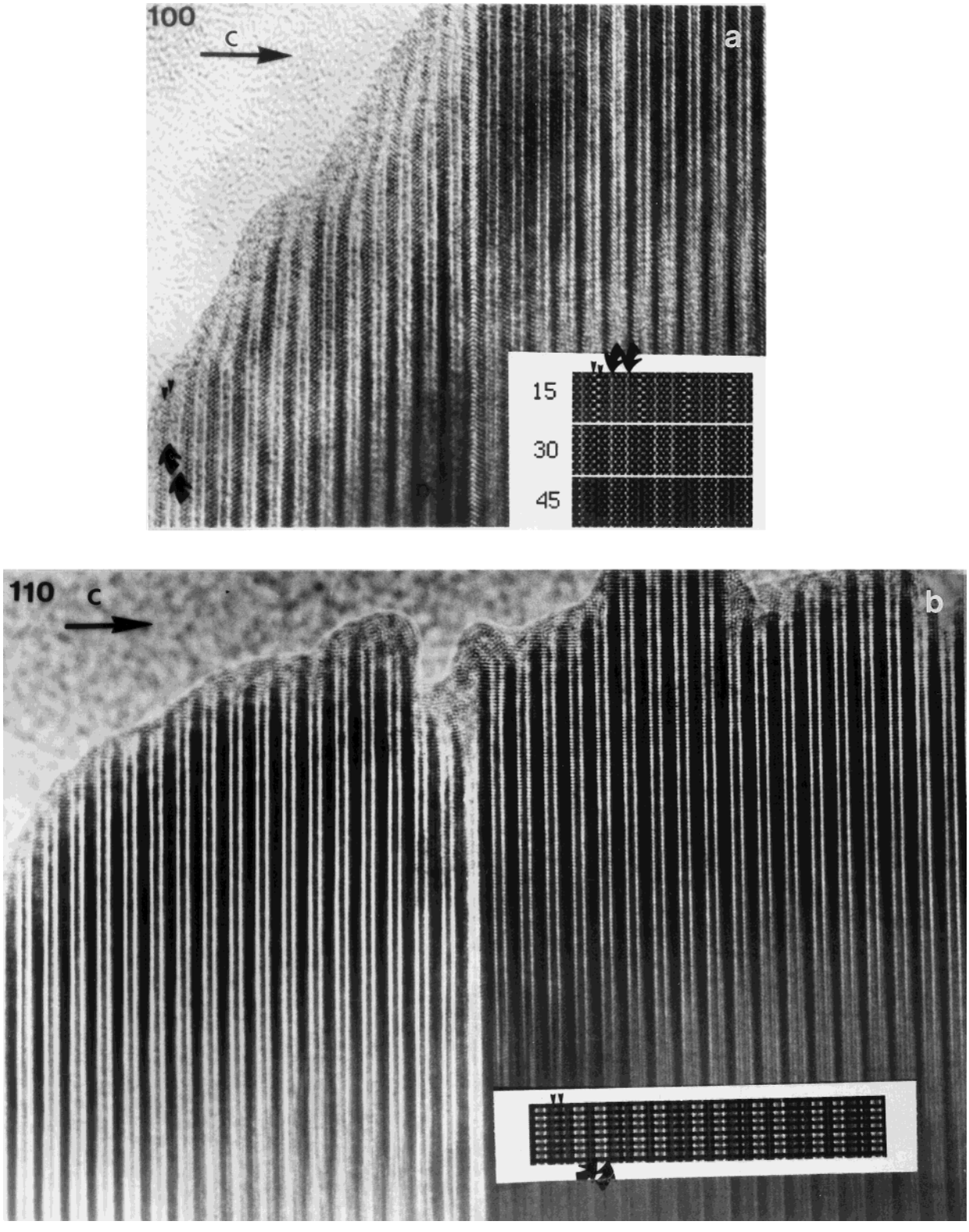

FIG. 6. (a) [100] and (b) [110] HREM images of $Ca_4Gd_2Cu_3O_8Cl_4$. In (a), the cations appear as dark dots. Inset shows the simulated images calculated for a focus value close to −250 Å and for three crystal thicknesses of 15, 30, and 45 Å. In (b), the calcium and chlorine atoms are imaged as bright dots. The calculated image for a focus value close to −550 Å is also shown.

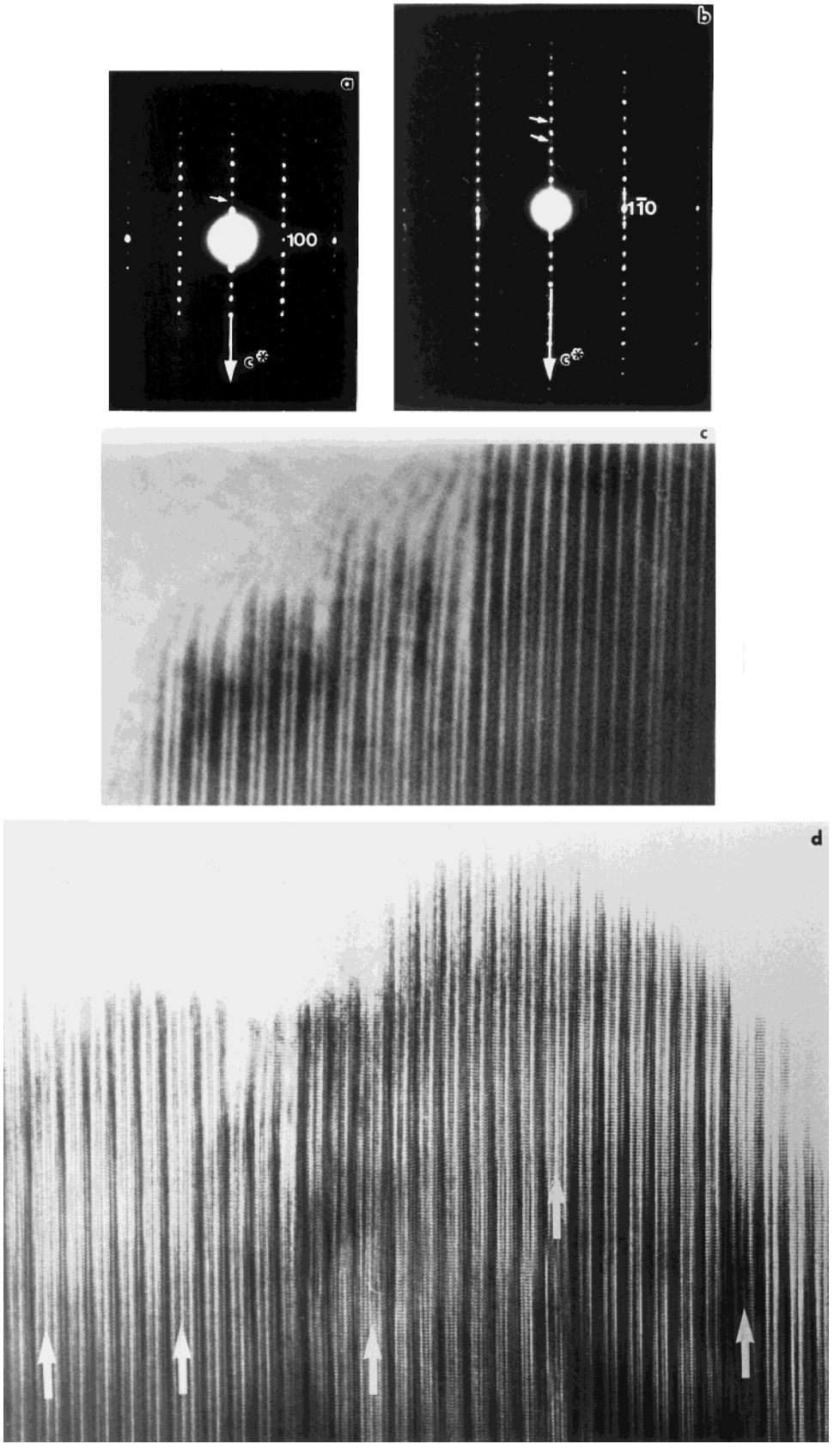

FIG. 7. (a) [100] and (b) [110] ED patterns showing streaks along c^*. (c) [100] corresponding image showing the coexistence of $Ca_4Gd_2Cu_3O_8Cl_4$ (on the left) and $Ca_2Gd_2Cu_2O_6Cl_2$ (on the right). (d) HREM image showing the higher member ($m = 2$ and $n = 1$) of the $(Ca_2CuO_2Cl_2)_m(Ca_2Gd_2Cu_2O_6Cl_2)_n$.

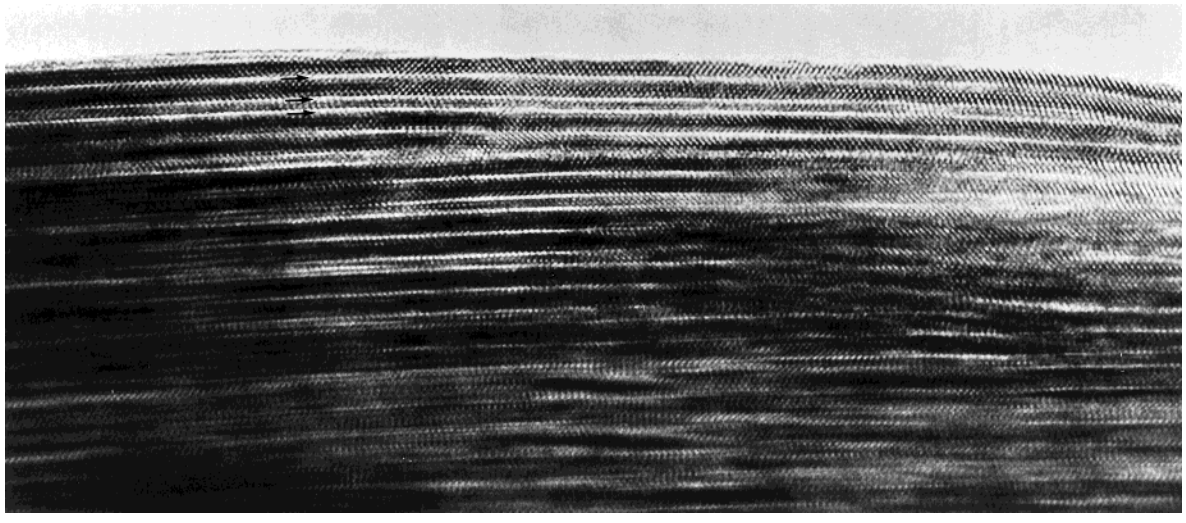

FIG. 8. HREM image showing the undulation of $[Ca_2Cl_2]_\infty$ layers.

1) matrix; they are indicated by large white arrows in Fig. 7d. These defective members are rather regularly separated by five or six adjacent $Ca_4Gd_2Cu_3O_8Cl_4$ members, forming polytypic microphases.

Cationic and anionic substitutions. The second origin of the disorder phenomena observed in these phases is due to short range substitutions. Two factors favor their formation: the ability of alkaline earth to be located in the $[Ln_2O_2]$ layers (8, 9) and the possibility that O locally substitutes for Cl. The strong differences between the corresponding interatomic distances, especially between Ca–O (≈2.5 Å) and Ca–Cl (3.3 Å), are accommodated through strong undulations of the layers. This feature arises in most of the crystals where distortions and contrast losses are observed at the level of the $[Ca_2Cl_2]_\infty$ layers. In a few cases, they are extended to larger areas leading to strongly disturbed crystals. As mentioned above, the EDS analyses evidence departure from the nominal composition. An example is given in Fig. 8. The undulation of the $[Ca_2Cl_2]_\infty$ layers is clearly observed by viewing the image at grazing incidence, and the adjacent layers are waving to compensate. In some places, these undulations are so intense that the layers coalesce according to a superdislocation mechanism.

CONCLUDING REMARKS

An intergrowth of the two limit structures, T and T*, corresponding to the member $m = n = 1$ of the structural series $(Ca_2CuO_2Cl_2)_m(Ca_2Ln_2Cu_2O_6Cl_2)_n$ (Ln = Gd, Sm), has been synthesized for the first time. Such a phenomenon is rather unusual, since the two end members exist, so that a disproportionation of this phase $Ca_4Ln_2Cu_3O_8Cl_4$ into $Ca_2CuO_2Cl_2$ and $Ca_2Ln_2Cu_2O_6Cl_2$ might be expected for thermodynamical reasons. This is the case for the oxides La_2CuO_4 (T) and $Ln_2Sr_{2-x}Ln'_xCu_2O_8$ (T*), for which no intergrowth has been observed to date. Such results open the route to the research of new other members in this series.

In fact, the actual average composition of the crystals, determined from the EDS analysis, shows a significant deviation from the ideal composition—e.g., "$Ca_{3.7}Gd_{2.3}Cu_{3.1}Cl_{3.8}$" instead of "$Ca_4Gd_2Cu_3Cl_4$"—due to the existence of nonstoichiometry involving both intergrowths mechanisms and local substitutions as demonstrated by HREM. These observations explain the relatively high B factors obtained from powder XRD data and the difficulty to lower the R factors.

This nonstoichiometry, as well on the ion substitutions already observed for the other oxychlorides without copper such as $Tl_2Ba_3O_5Cl_2$ (10), emphasize the high flexibility of those frameworks and suggest that the different members of the family could be stabilized by controlling carefully the experimental conditions and the chemical compositions.

ACKNOWLEDGMENT

This work was supported by IFCPAR (Indo French Centre for the Promotion of Advanced Research), Contract 808.1.

REFERENCES

1. M. Al-Mamouri, P. P. Edwards, C. Greaves, and M. Slaski, *Nature* **369,** 382 (1994).
2. Z. Hiroi, N. Kobayashi, and M. Takano, *Natue* **371,** 139 (1994).

3. B. Grande and Hk. Müller-Buschbaum, *Z. Anorg. Allg. Chem.* **417,** 68 (1975); and **429,** 88 (1977).
4. R. L. Fuller and M. Greenblatt, *J. Solid State Chem.* **92,** 386 (1991).
5. J. Rodriguez-Carvajal, *in* ''Abstracts of the Satellite Meeting on Powder Diffraction of the XV Congress of the IUCR, Toulouse, France, 1990, p. 127.
6. K. V. Ramanujachary, M. Greaney, R. L. Fuller, and M. Greenblatt, *J. Solid State Chem.* **93,** 263 (1991).
7. M. Huvé, C. Martin, A. Maignan, C. Michel, and B. Raveau, *J. Solid State Chem.* **114,** 230 (1995).
8. J. Akimitsu, S. Suzuki, M. Watanabe, and H. Sawa., *Jpn. J. Appl. Phys.* **27,** L1859 (1988).
9. E. Takayama-Muromachi, Y. Matsu, Y. Uchida, F. Izumi, M. Onoda, and K. Kato, *Jpn. J. Appl. Phys.* **27,** L2283 (1988).
10. F. Letouzé, C. Martin, D. Pelloquin, C. Michel, M. Hervieu, and B. Raveau, *Mater. Res. Bull.* **31**(7), 773 (1996).